156

Combustion Synthesis in the Ti-C-Ni-Mo System: Part II. Analysis

J.C. LaSALVIA and M.A. MEYERS

Combustion-wave arrest experiments provide the means of greater understanding of the physical phenomena which occur during the propagation of a combustion wave within a Ti-C-Ni-Mo powder mixture. The apparent activation energy for the process ($E \approx 120 \pm 40$ kJ/mol) and the observations reported in the companion article indicate that the rate-limiting step in the reaction between Ti and C is the dissolution of C into the Ti-Ni-C melt. Temperature profile analysis indicates that the 2 μm C flakes are completely consumed within approximately 0.2 seconds. The formation of TiC_x spherules and their subsequent detachment is explained in terms of compressive stresses established in the growing TiC_x layer on the C particle. The compressive stresses are estimated to exceed 1 GPa, and an energy balance analysis predicts the formation of spherules for layer thicknesses on the order of 1 μm, consistent with the experimental results.

I. INTRODUCTION

IN the companion article,[1] the micromechanisms (*e.g.*, phase and structural transformations, capillary spreading, product formation and coarsening, *etc.*) of self-propagating high-temperature synthesis in a Ti-C-Ni-Mo powder mixture, using the quenching technique developed by Rogachev *et al.*,[2] were examined. The utility of this technique for examining physical processes on the microscale which occur within the three general regions (*i.e.*, unreacted, partially reacted, and fully reacted regions) of a combustion wave has been previously demonstrated (and advocated).[2–10] However, this technique does not allow quantification of reaction rates, degree of conversion, and temperature as a function of time or space within these regions. Information such as this further enhances the understanding of the physical processes and their relative importance to the propagation of a stable combustion wave.[10–13] The primary focus of this article is to rationalize the observations reported in the companion article[1] and to correlate them with the micromechanisms. Calculations leading to quantification of the parameters responsible for the key features of the mechanism of spherule formation are presented.

II. APPARENT ACTIVATION ENERGY DETERMINATION

The companion article[1] contains information on powder preparation, as well as on the combustion-wave velocity and temperature measurement technique and data. An expression for the velocity of propagation of a stable planar combustion wave in terms of the adiabatic temperature, activation energy for the reaction, and thermophysical properties has been previously derived.[14,15,16] The equations which describe the propagation of a planar "gasless" combustion wave traveling in an isotropic, homogeneous medium are[16]

$$\frac{\partial T}{\partial t} = \alpha \frac{\partial^2 T}{\partial x^2} + \frac{Q}{C_p} \frac{\partial \eta}{\partial t} \qquad [1]$$

$$\frac{\partial \eta}{\partial t} = K_0 (1 - \eta)^n e - (E/RT) \qquad [2]$$

where T is the temperature, α is the thermal diffusivity, Q is the heat of reaction, C_p is the heat capacity, K_0 is the reaction-rate constant, n is the order of the reaction, R is the universal gas constant, and E is the activation energy for the reaction. Equation [1] also assumes constant thermophysical properties and negligible heat losses to the surroundings. Based upon some simplifying approximations (*e.g.*, "narrow" zone), Eqs. [1] and [2] can be solved to obtain the following expression for the velocity of a stable planar combustion wave:[16]

$$U = \sqrt{\sigma_n K_0 \alpha \left[\left(\frac{C_p T_{ad}}{Q}\right)\left(\frac{RT_{ad}}{E}\right)\right] \exp\left(\frac{-E}{RT_{ad}}\right)} \qquad [3]$$

where U is the combustion-wave velocity, σ_n is a constant which depends upon the order of the reaction (*e.g.*, for $n = 0$, 1, and 2, $\sigma_n = 2$, 1.1, and 0.73, respectively[16]), and T_{ad} is the adiabatic temperature. The apparent activation energy E for the reaction is the slope of the graph obtained by plotting $\ln [(T_{ad} - 298)U^2/T_{ad}^2]$ as a function of $1/T_{ad}$.

Figure 1 is a plot of $\ln [(T_{ad} - 298)U^2/T_{ad}^2]$ as a function of $1/T_{ad}$ for the data reported in the companion article (*i.e.*, curve 3 in Figure 3 of Reference 1). The apparent activation energy obtained is $E \approx 120 \pm 40$ kJ/mol. The large error is due mainly to the uncertainty in the actual combustion-wave temperatures (*i.e.*, $\delta T \approx 400$ K). This corresponds very nearly to the activation energy of C dissolution in the Ti melt (*i.e.*, 117 kJ/mol).[17] Dunmead *et al.*[18] obtained an apparent activation energy of 133 ± 50 kJ/mole for the Ti-C-Ni system. Within the experimental error, the addition of Mo does not appear to affect the rate-limiting mechanism of reaction in the Ti-C-Ni system for the compositions investigated. This is consistent with the micromechanistic results obtained in the companion article,[1] where it was observed that the Ti-C interaction results in the formation

J.C. LaSALVIA, Postdoctoral Fellow, Institute for Mechanics and Materials, and M.A. MEYERS, Professor, Department of Applied Mechanics and Engineering Sciences, are with the University of California, San Diego, CA 92093.

Manuscript submitted October 24, 1994.

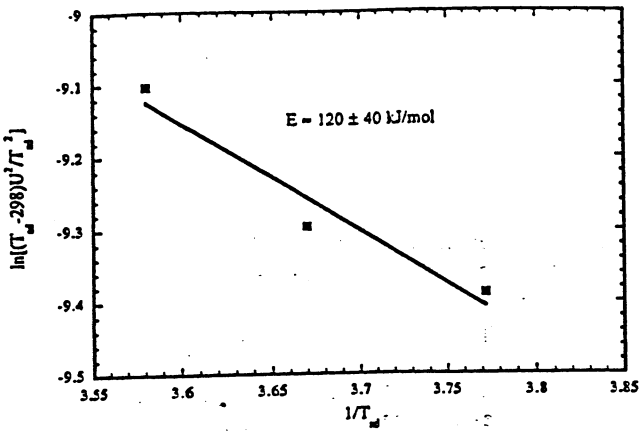

Fig. 1—Arrhenius plot for combustion-wave propagation in a Ti-C-Ni-Mo powder mixture; slope is the activation energy for the process.

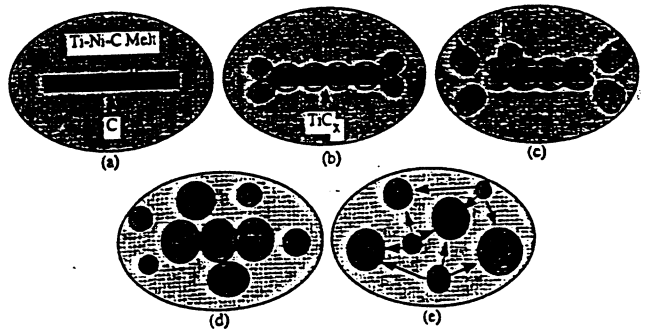

Fig. 2—Sequence of formation of TiC_x spherules. (*a*) C particle enveloped by Ti-Ni-C melt; (*b*) nucleation and growth of TiC_x precipitates; (*c*) further growth and initial formation of TiC_x spherules from C particle edges, and nucleation and growth of new TiC_x grain at the intersection of the initial TiC_x grains with the Ti-Ni-C melt; (*d*) formation of TiC_x chain due to TiC_x/C interface migration, and residual C within these grains; and (*e*) separation of TiC_x chain into individual spherules, and growth by "Ostwald ripening."

of a TiC_x layer which continually ejects into the Ti-Ni-C melt TiC_x spherules with sizes on the order of 1 μm. This prevents kinetic "braking" of the reaction by continually exposing the C particle surface to the melt, thus ensuring a high reaction rate.

III. MICROMECHANISMS FOR COMBUSTION SYNTHESIS

A. *General Discussion*

Figure 2 is a schematic illustration of the processes resulting in the formation of the TiC_x spherules which were observed in the companion article.[1] After the Ti-Ni melt becomes saturated (or supersaturated) with C, heterogeneous nucleation and growth of TiC_x precipitates on the C particles occur, as shown in Figure 2(b). Nucleation is favored at sites which have high excess free energy such as defects (*i.e.*, dislocations) and ledges.[19] It is generally observed that the TiC_x spherules which form first do so at the edges of the C particles. These TiC_x spherules form first because their growth rates are higher than the ones away from the edges due to the larger surface area per unit volume at the edge sites. Some TiC_x spherules that have separated from the TiC_x layer appear to have been formed by nucleation and growth processes at the intersection of the existing TiC_x precipitates and Ti-Ni-C melt. These sites seem to suggest the importance of C diffusion through the existing TiC_x precipitate boundaries into the Ti-Ni-C melt. Both processes are shown in Figure 2(c). The processes shown in Figure 2(c) occur when the C particle size is large with respect to the TiC_x spherule size. However, for C particle sizes on the order of the TiC_x spherule size, the process of continuous TiC_x spherule formation by breakup of the TiC_x layer does not occur. The final consumption of the C particles results in the formation of the "rosary" structure, as shown in Figure 2(d). The TiC_x spherules in the rosary structure pinch off at existing precipitate boundaries and are carried into the Ti-Ni melt. Spherule coarsening occurs by dissolution reprecipitation, as shown in Figure 2(e).

It is important to realize that the mechanism by which the TiC_x spherules are formed depends upon the C particle size. Borovinskaya *et al.*[10] found three different mechanisms based upon the following general C particle sizes: (1) $r_c < 1$ μm, (2) 1 μm $< r_c <$ 10 μm, and (3) $r_c >$ 10 μm. For the case where r_c is less than 1 μm, no TiC_x layer is formed on the C particle. Instead, the C particle completely dissolves into the Ti-Ni melt. TiC_x is homogeneously nucleated as the melt cools below the liquidus line in the phase diagram for the Ti-C-Ni ternary system. For 1 μm $< r_c <$ 10 μm, a TiC_x layer is formed on the C particle. This layer does not break up into TiC_x spherules until the C particle has been consumed (*i.e.*, rosary structure formation). Finally, for $r_c >$ 10 μm, the TiC_x layer undergoes a process of continuous formation and breakup into TiC_x spherules. This process continues until the residual C particle is on the order of the TiC_x layer, thickness at which time, mechanism (2) becomes active. Because of the distribution in the sizes of the C particles used in this investigation, mechanisms (2) and (3) appear to be prevalent.

The formation and growth of the TiC_x layer, as well as the cusplike features, can be interpreted in terms of either the reaction diffusion or dissolution-reprecipitation mechanism. The reaction diffusion mechanism postulates that a dynamic equilibrium is created in which the TiC_x dissolution at the TiC_x/Ti-Ni melt interface and TiC_x formation at the TiC_x/C interface balance one another such that the TiC_x layer thickness δ remains constant with time. This requires simultaneous diffusion of both C and Ti. However, Ti diffusion in TiC is several orders of magnitude slower than C diffusion. According to Sarian,[20] the diffusion coefficients for Ti and C diffusing through TiC are approximately given by (neglecting compositional variation)[20,21]

$$D_{Ti}^{TiC} \approx (9 \times 10^{12}) \exp\left(\frac{-175{,}000}{RT}\right) (\mu m^2/s) \quad [4]$$

$$D_{C}^{TiC} \approx (5.75 \times 10^{8}) \exp\left(\frac{-96 \times 10^{3}}{RT}\right) (\mu m^2/s) \quad [5]$$

where R is the universal gas constant (1.987 cal/mol K) and T is the absolute temperature. Assuming a temperature of approximately 2700 K to determine the diffusion coefficients for Ti and C in TiC given by Eqs. [4] and [5], respectively, the diffusion distances for both Ti and C can be estimated by[22]

$$\delta_i = 2\sqrt{D_i^{TiC} t} \quad [6]$$

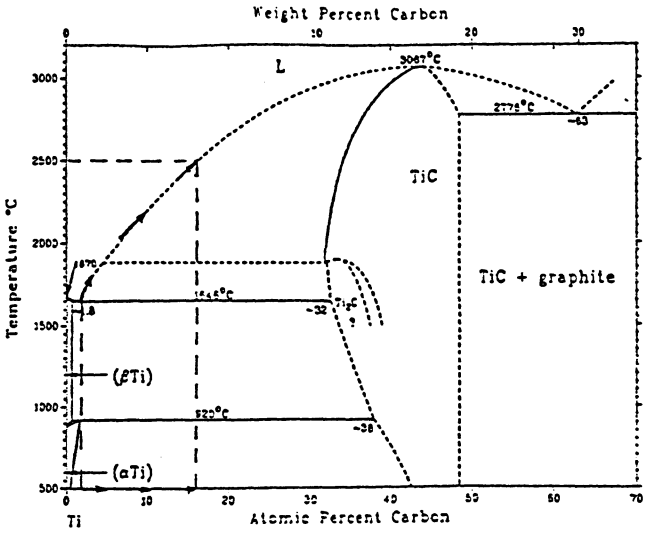

Fig. 3—Ti-C binary phase diagram.[23]

$$\delta_{Ti} = 2\sqrt{(7.6 \times 10^{-2}\ \mu m^2/s)\ (0.2\ s)} \approx 0.24\ \mu m \quad [7a]$$

$$\delta_C = 2\sqrt{(11\ \mu m^2/s)\ (0.2\ s)} \approx 2.9\ \mu m \quad [7b]$$

Even near the adiabatic temperature, the diffusion distance for C is 12 times greater than for Ti (at 2000 K, it is 155 times greater). This result indicates that Ti bulk diffusion may be negligible, and as a consequence, the reaction-diffusion mechanism is not plausible. Therefore, the dissolution-reprecipitation mechanism will be discussed in detail.

B. *Dissolution-Reprecipitation Mechanism*

The dissolution-reprecipitation mechanism of formation proceeds by the dissolution of C into the Ti-Ni melt followed by its saturation with C and then heterogeneous nucleation of TiC_x precipitates on the C particles. The precipitates link up to form a solid TiC_x layer. The reaction between Ti and C continues by C diffusing through the TiC_x layer, dissolving into the Ti-Ni-C melt, and reprecipitating at the TiC_x/melt interface as TiC_x.

Due to the high heating rate in the combustion wave, the reaction between Ti and C powders essentially starts upon melting of the Ti particles which, according to the Ti-C phase diagram shown in Figure 3, occurs at approximately 1939 K.[23] It is assumed that the subsequent capillary spreading and enveloping of the C particles by the Ti-Ni melt is extremely rapid. Melt spreading appears to be aided by the spontaneous formation of a TiC_x layer on the C particle (*i.e.*, spreading occurs on the TiC_x layer and not C surface).[7] During the reaction, assuming adiabatic conditions, the temperature rises to approximately 2800 K. This temperature is considerably lower than the melting point of TiC (~3340 K), and as a result, the TiC_x product formed is in the solid state. The solubility of C within the Ti-Ni melt follows the arrows on the liquidus line, as shown in Figure 3. Near the melting point of Ti, it is approximately 3 at. pct, while at the adiabatic temperature, it is approximately 16 at. pct. Thus, upon Ti-Ni melt formation, C will enter into solution by dissolution. Once the C concentration within the Ti-Ni melt exceeds the solubility limit, the formation of TiC_x by precipitation becomes thermodynamically favorable. The composition of the TiC_x precipitates

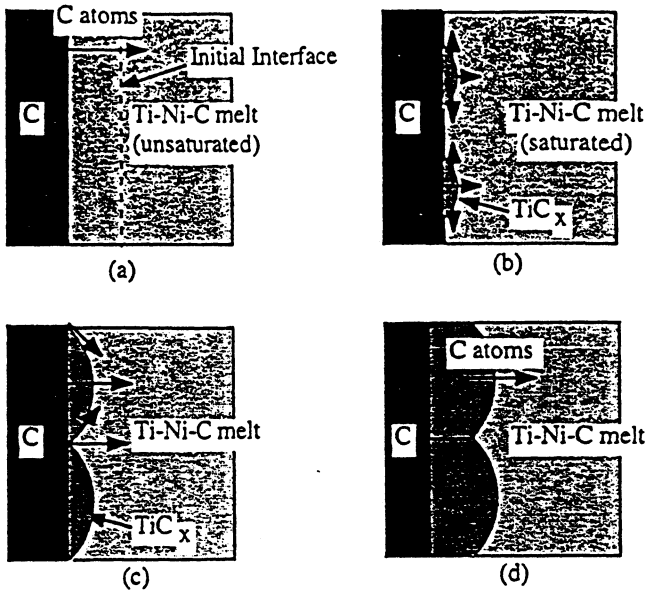

Fig. 4—Formation of TiC_x precipitates on C by the dissolution-reprecipitation mechanism. The Ti diffusion is negligible. (*a*) Dissolution of C into the Ti-Ni melt; (*b*) saturation of Ti-Ni-C melt with C and precipitation of TiC_x on C; (*c*) impingement of TiC_x precipitates and formation of layer; and (*d*) growth of TiC_x layer.

can be estimated by assuming that the composition which forms first will be the one which is in equilibrium with the saturated melt. From Figure 3, this would be $TiC_{0.47}$. Precipitation at the surface of C is preferred because of the lower activation energy for heterogeneous nucleation. The rate of heterogeneous nucleation has been shown by Fine[24] to be many orders of magnitude higher than that of homogeneous nucleation. Growth parallel to the C surface is initially faster than growth perpendicular to it, since the C concentration within the Ti-Ni melt near the surface of the C particle will be high. As these TiC_x precipitates grow, they eventually impinge upon one another and lateral growth is arrested, whereas growth perpendicular to the C surface continues. Once the surface of the C particle has been completely covered by the TiC_x layer, consumption of C is limited by dissolution of C into the Ti-Ni melt and not by C diffusion through the TiC_x layer; this is consistent with activation energy calculation. Due to the reaction between Ti and C, the local temperature increases and, consequently, the C concentration necessary for saturation increases within the Ti-Ni melt (Figure 3). Thus, for further TiC_x formation, it is necessary for the Ti-Ni melt to again become enriched with C. This occurs by C diffusion through the TiC_x layer and its subsequent dissolution into the Ti-Ni melt (*i.e.*, once the composition of the TiC_x layer in contact with the Ti-Ni melt exceeds the equilibrium level, it will dissolve). This process of dissolution of C into the Ti-Ni melt and subsequent reprecipitation of TiC_x at the TiC_x layer/Ti-Ni melt interface continues until the C is consumed. This process is shown schematically in Figure 4.

Based upon a simple model, the approximate time it takes to fully consume a C particle (*i.e.*, flake) can be estimated. Figure 5 illustrates the model used to make the calculation. A single C particle and Ti-Ni melt comprise a reaction cell. It is assumed that the rate of reaction is determined by C diffusion through the forming TiC layer. The following additional assumptions are made:

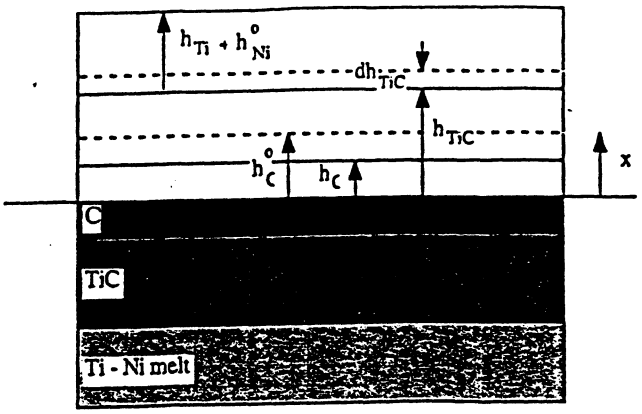

Fig. 5—One-dimensional reaction cell used to model the reaction kinetics.

(1) quasi-isolated system;
(2) one-dimensional approximation;
(3) the C concentration gradient in the TiC layer is both linear and time independent;
(4) heat is evolved at the TiC/Ti-Ni interface;
(5) thermophysical properties are constant (*i.e.*, averaged values); and
(6) the temperature of the cell is uniform.

During the reaction, the temperature of the cell can be assumed to be uniform because the thermal diffusion distance is several orders of magnitude greater than the thickness of the C particles (approximate characteristic size of cell). The thermal diffusion distance Δ_{th} can be estimated from the solution to the one-dimensional heat-transfer problem of a semi-infinite medium whose surface temperature is suddenly increased. The thermal diffusion distance Δ_{th} is given by[25]

$$\Delta_{th} = \sqrt{12\left(1 - \frac{T}{T_0}\right)\alpha_C t_2} \qquad [8]$$

$$\Delta_{th} = \sqrt{12(0.001)\ (20\ \text{mm}^2/\text{s})\ (0.2\ \text{s})} \approx 0.2\ \text{mm} = 200\ \mu\text{m}$$

where it was assumed that the difference in temperature between two points Δ_{th} apart is only 0.1 pct and α_C is the thermal diffusivity of C ($\alpha_C \approx 20\ \text{mm}^2/\text{s}$[25]). Assuming the C particle thickness to be 0.20 μm (Figures 9(c) and 11(c) in the companion article[1]), the thermal diffusion distance is approximately 1000 times larger.

Based upon the model illustrated in Figure 5 and the conservation of mass, the growth rate of the TiC layer $\dot{h}_{TiC}$ is related to the rate of consumption of the C particle $\dot{h}_C$ by

$$\dot{h}_{TiC} = -\left(\frac{\rho_C}{\rho_{TiC}}\right)\left[\frac{(MW)_{TiC}}{(MW)_C}\right]\dot{h}_c \qquad [9]$$

where ρ_C is the density of C, ρ_{TiC} is the density of TiC, $(MW)_C$ is the molar weight of C, and $(MW)_{TiC}$ is the molar weight of TiC. Here, it is assumed that the C transported across the TiC layer reacts immediately with Ti at the TiC/Ti-Ni melt interface to form TiC. The heating rate $\dot{Q}$ (*i.e.*, energy release rate) is simply given by

$$\dot{Q} = \rho_{TiC} A_C Q \dot{h}_{TiC} = -\left[\frac{(MW)_{TiC}}{(MW)_C}\right]\rho_C A_C Q \dot{h}_C \qquad [10]$$

where A_C is the area of the C particle and Q is the heat of reaction. From the conservation of energy, the rate of change of temperature is given by

$$\dot{T} = \frac{\dot{Q}}{\sum_i m_i C_{P_i}}$$

$$\dot{T} = \frac{-(MW)_{TiC}\, Q\dot{\phi}}{\left[(MW)_C C_{P_C} + (MW)_{Ti} C_{P_{Ti}} - (MW)_{TiC} C_{P_{TiC}}\right]\phi + (MW)_{TiC} C_{P_{TiC}} + x_{Ni}\,(MW)_{Ni}\, C_{P_{Ni}}} \qquad [11]$$

where $\phi = h_C/h^0_C$ (*i.e.*, normalized C thickness), h^0_C is one-half the initial thickness of the C particle, C_{P_i} is the heat capacity of the ith component, m_i is the mass of the ith component, and x_{Ni} is the mole fraction of Ni. Integrating Eq. [11] yields

$$T = T_0 + \left[\frac{B_1}{B_2}\right]\ln\left[\frac{B_2 + B_3}{B_2\phi + B_3}\right] \qquad [12a]$$

$$B_1 = (MW)_{TiC} Q \qquad [12b]$$

$$B_2 = (MW)_C C_{P_C} + (MW)_{Ti} C_{P_{Ti}} - (MW)_{TiC} C_{P_{TiC}} \qquad [12c]$$

$$B_3 = (MW)_{TiC} C_{P_{TiC}} + x_{Ni}\,(MW)_{Ni} C_{P_{Ni}} \qquad [12d]$$

where T_0 is the initial temperature. Equation [12a] expresses the temperature of the reaction cell as a function of the normalized thickness of the C particle. Consistent with the continuum combustion models, the reacted fraction or degree of conversion $\eta = 1 - \phi$. The rate of consumption of C, ϕ, is determined by considering the conservation of mass. The rate of change of mass of C is simply equal to the mass of C atoms diffusing across the TiC layer per second. Thus, using Fick's first law, the rate of consumption of C is given by

$$\dot{\phi} = \frac{1}{N_{Av0}}\left[\frac{(MW)_C}{\rho_C h^0_C}\right] D^{TiC}_C \frac{d[C]}{dx} \qquad [13]$$

where N_{Av0} is Avogadro's number, D^{TiC}_C is the diffusion coefficient of C in TiC, and $d[C]/dx$ is the concentration gradient of C in the TiC layer. Equation [13] can be rewritten as

$$\frac{d(1-\phi)^2}{dt} = B_4 D^{TiC}_C \qquad [14a]$$

$$B_4 = \frac{-2}{N_{Av0}}\left(\frac{N_C}{a_0^3}\right)\left[\frac{\rho_{TiC}}{(MW)_{TiC}}\right]\left[\frac{(MW)_C}{\rho_C h^0_C}\right]^2 \frac{d\beta}{d\zeta} \qquad [14b]$$

where N_C is the number of C atoms in a TiC lattice cell, a_0 is the TiC lattice parameter, and $d\beta/d\zeta$ is the normalized C concentration gradient within the growing TiC layer. Based upon the values for the thermophysical properties, an approximate analytical solution to the preceding equations is possible. However, because of the nonlinear dependence of D^{TiC}_C on temperature, the error introduced by the approximation necessary to obtain the analytical solution is substantial. It is trivial to use numerical means to solve the preceding equations. The following values were used for the various constants in the model:[26,27,28] $a_0 = 4.3$ Å, $N_C \approx 4$, $d\beta/d\zeta \approx -0.5$, $x_{Ni} = 0.4374$ (*i.e.*, 30 wt pct),

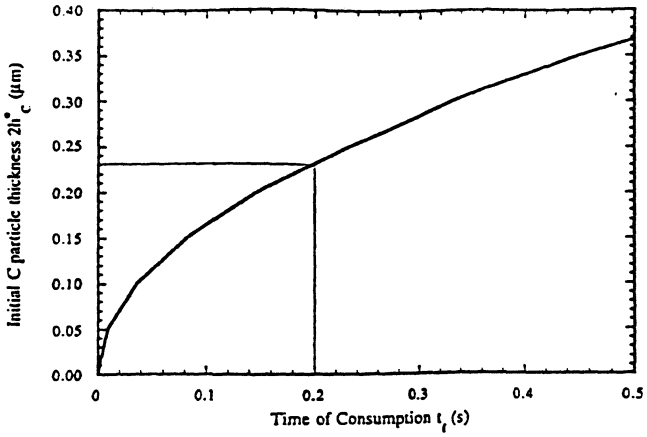

Fig. 6—Variation of initial thickness $2h^0_C$ as a function of time of C consumption t_f.

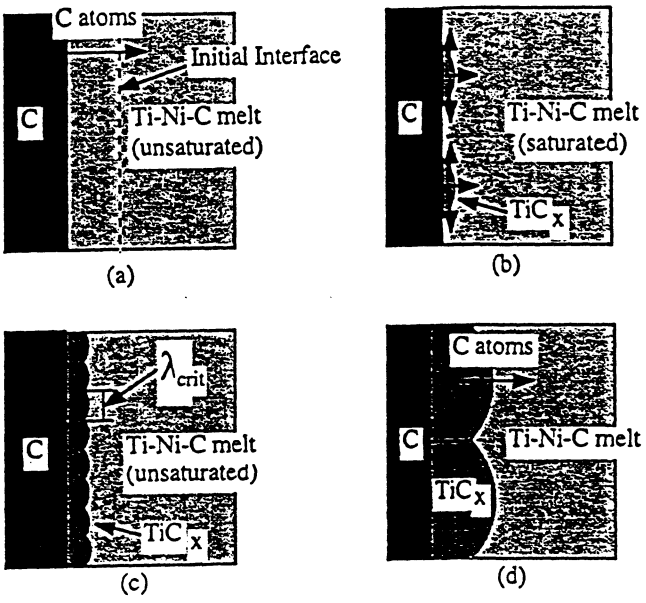

Fig. 7—Formation of cusped TiC_x layer on C particle due to minimization of strain energy. (*a*) Dissolution of C into the Ti-Ni melt, and diffusion of Ti into C particle; (*b*) heterogeneous nucleation of TiC_x precipitates; (*c*) roughening of TiC_x layer due to strain energy; and (*d*) growth of TiC_x phase.

ρ_C = 2.2 g/cm³, $\rho_{Ti} \approx$ 4.5 g/cm³, $\rho_{TiC} \approx$ 4.9 g/cm³, ρ_{Ni} = 8.9 g/cm³, C_{PC} = 2.14 J/g K, C_{PTi} = 0.987 J/g K, C_{PTiC} = 1.051 J/g K, C_{PNi} = 0.663 J/g K, $(MW)_C$ = 12.011 g/mol, $(MW)_{Ti}$ = 47.88 g/mol, $(MW)_{TiC}$ = 59.89 g/mol, $(MW)_{Ni}$ = 58.69 g/mol, $Q \approx$ 1141 J/g, and T_0 = 1939 K. It was assumed that the reaction does not occur until the Ti-Ni melt has formed (consistent with observations). The energy required to raise the temperature of the reaction cell to 1939 K and to form the Ti-Ni melt is also assumed to be transferred from the surroundings. This amount of energy is further assumed to be transferred out of the reaction cell (*e.g.*, absorbed by neighboring reaction cells) so that the adiabatic temperature, as determined in the companion article,[1] is not exceeded. Figure 6 is a plot of the time for complete consumption of the C particle in the reaction cell as a function of its initial thickness. As expected, the time for consumption is proportional to the square of the initial thickness. For an initial thickness of 0.23 μm, the predicted time for consumption is approximately 0.2 seconds. As was observed in the companion article,[1] this value is the approximate thickness of the C particles. While this result is consistent with the experimentally derived time of C particle consumption, it seems to suggest that C diffusion through the TiC_x layer is rate limiting. However, the curve, as shown in Figure 6, should be interpreted as an upper bound for the time of consumption because of the adiabatic assumption. Initially, the rate of change of the reaction cell temperature is low because the value for E/RT in Eq. [5] is large. Only when the temperature is sufficiently high such that E/RT is small does the temperature rise rapidly. Therefore, one expects that initially the temperature rise is dominated by heat conduction.

C. *TiC_x Layer Cusp Formation*

A cusped layer is intermediate between the initial flat continuous layer and the formation of spherules. Two possible explanations for the formation of the cusplike features exhibited by the TiC_x layer are examined. The first explanation is based on nucleation and growth kinetics. The width of the cusps (*i.e.*, wavelength) is determined by both the heterogeneous nucleation rate and subsequent lateral growth rate. Figures 7(c) and (d) schematically illustrate this process. The higher the nucleation rate for a given lateral growth rate, the shorter the wavelength. Conversely, the higher the lateral growth rate for a given nucleation rate, the longer the wavelength. The morphological changes are governed solely by minimization of surface energy.

The second explanation for the formation of the cusplike features is due to the minimization of the total strain energy. This phenomenon is called "roughening" and has been observed in heteroepitaxial thin film growth.[29] Strain energy can arise due to differences in the thermal expansion behavior, lattice mismatch between the TiC_x layer and C substrate, or compositional variation throughout the TiC_x layer. It is important to specify in this case that it is assumed that the rate of strain energy increase is much greater than its decrease due to strain relaxation by dislocation motion and diffusion processes. Because of the high temperatures experienced during the reaction, neglecting strain relaxation due to diffusion processes is a limitation of this model. It is uncertain to what extent diffusion processes are able to relax the strain energy buildup. However, morphological changes are the result of diffusion processes. The formation of the TiC_x layer proceeds as shown in Figure 7; in this case, the layer is initially planar. As the layer thickens, the total strain energy within the layer increases. Eventually, the thickness of the layer is such that it is energetically favorable to form the cusps. Chiu and Gao[30] have shown that the overall energy of the layer (strain plus surface) is decreased by the formation of the cusps. The strain energy becomes concentrated at the cusps, while the material away from the cusps becomes "unloaded." The formation of the cusps does increase the overall interfacial energy by increasing the total interface area; however, the decrease in total strain energy is sufficient to compensate this increase, resulting in a decrease in the overall energy of the layer.

The analytical results by Chiu and Gao[30] show that there is a critical wavelength for the cusps below which the increase in surface energy dominates and dampens the for-

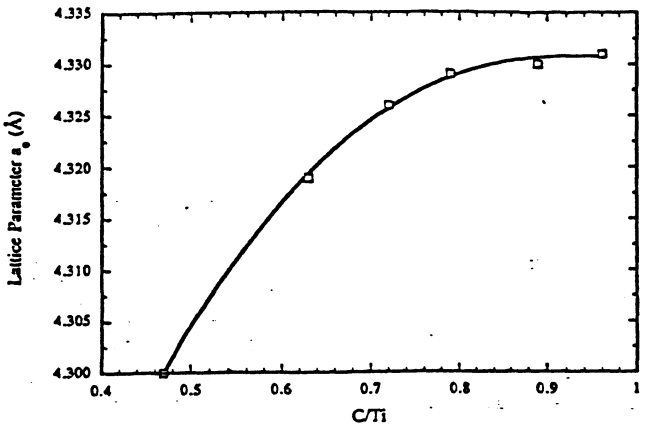

Fig. 8—Variation of TiC_x lattice parameter with stoichiometric ratio.[26]

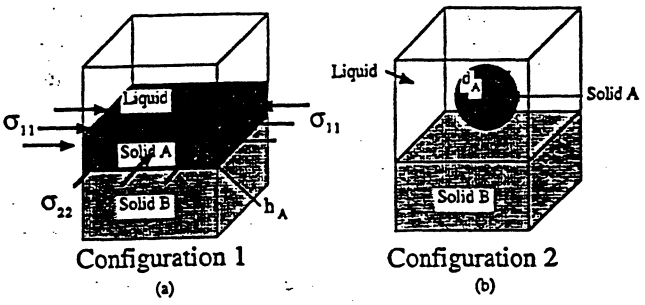

Fig. 9—Simplified model configuration used to show the destabilizing effect of strain energy on system configuration.

mation of the cusps. Above this critical wavelength, the decrease in the strain energy dominates and drives the formation of the cusps. The critical wavelength for the initial instability is given as[30]

$$\lambda_{cr} = \frac{\pi}{2}\left(\frac{\gamma}{w_0}\right) \qquad [15]$$

where λ_{cr} is the critical wavelength (m), γ is the interfacial surface energy density (J/m²), and w_0 is the strain energy density (J/m³). Equation [15] shows that the critical wavelength for the initial destabilization of a flat surface is inversely proportional with the strain energy density. This result will be compared in Section D with the analytical prediction for the critical layer thickness for TiC_x spherule formation.

D. *TiC_x Spherule Formation: Analysis*

In this analysis, it will be assumed that the formation of TiC_x spherules is due to minimization of strain energy within the TiC_x layer and not surface energy. It is further assumed that the basis for the strain energy within the TiC_x layer is the variation of TiC_x lattice parameter as a function of composition, as shown in Figure 8.[26]

A simple analytical expression can be derived based upon an energetic analysis to show the potential effect of both surface and strain energy on the stability of a planar layer. Consider the two configurations shown in Figure 9. In Figure 9(a), it is assumed that the solid phase A forms an incoherent layer of thickness h_A on solid phase B as a result of a chemical reaction between the liquid and B. In Figure 9(b), A exists as a spherical particle within the liquid phase. In the following analysis, the following additional assumptions are made.

(1) During growth, a plane state of stress is generated within A due to compositional variation through the layer.
(2) All interfacial energies are assumed to be isotropic, and the interfacial energies between A and B and between B and the liquid are equal.
(3) Both A and B are linear elastic and isotropic bodies; strain relaxation by diffusion and generation of interfacial dislocations is neglected.
(4) In configuration 2, A may be residually strained due to only a partial relaxation of the initial compositional inhomogeneity.
(5) The chemical energy of A in both configurations is the same.
(6) The thickness of A determines the size of the spherical particle formed due to the minimization of the diffusion length.

It is assumed in (3) that strain relaxation does not occur to a sufficient degree to affect substantially the magnitude of the strain. This implies that the rate of dislocation generation and subsequent glide is negligible compared with the growth rate. It has been observed experimentally during the growth of thin films that strain relaxation due to roughening can occur before dislocations will be spontaneously generated within the film.[31] In (4), it is assumed that after the formation of the spherule, the strain energy decreases due to compositional homogenization. The justification for assumption (6) will be presented later.

Based upon assumptions (2) through (5), the free energy difference ΔG between configurations 2 and 1 is given by

$$\Delta G = G_2 - G_1 = -\bar{w}_0 (1 - f) V_A + (A_2 - A_1)\gamma \qquad [16]$$

where $\bar{w}_0$ is the average strain energy density contribution to the free energy of A in configuration 1, f is the fraction of the average strain energy density $\bar{w}_0$ of A in configuration 2, V_A is the volume of A (equal in both configurations), γ is the surface energy density of A relative to the liquid, A_1 and A_2 are the surface areas of A in configurations 1 and 2, respectively. Equation [16] can be rewritten as

$$\Delta G = -\bar{w}_0 A_1 \left\{(1 - f) h_A - \left[\left(\frac{36\pi}{A_1}\right) 1/3\ h_A\ 2/3 - 1\right]\left(\frac{\gamma}{\bar{w}_0}\right)\right\} \qquad [17]$$

where $A_2 = (36\pi)^{1/3}(A_1 h_A)^{2/3}$. The critical thickness h_A^* for which configuration 2 would be favored over configuration 1 is obtained by setting ΔG in Eq. [17] equal to zero. From Eq. [17], and assuming that $A_1 = h_A^2$ (a cube geometry for the layer minimizes the mass transport distance required for morphological change), the critical thickness h_A^* is given by

$$h_A^* = \frac{3.836}{1 - f}\left(\frac{\gamma}{\bar{w}_0}\right) \qquad [18]$$

The interfacial energy density γ for most solid-liquid systems is typically on the order of 1 J/m².[32] Comparing Eq. [18] with [15] shows that this simple analysis yields a result which is comparable.

The principal stresses for a plane state of stress are re-

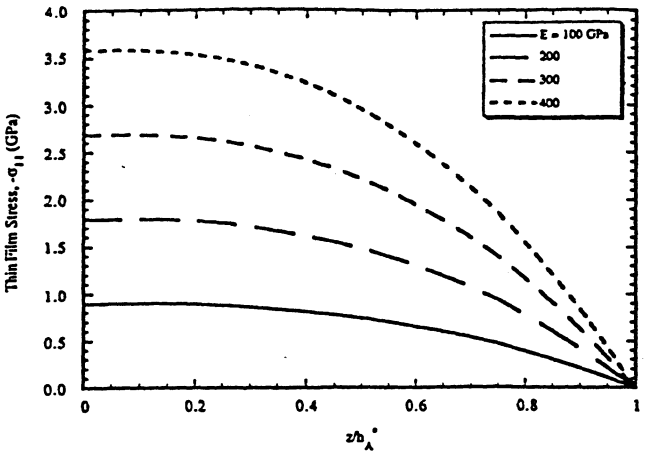

Fig. 10—Thin film stress for various values of Young's modulus E; ν = 0.2.

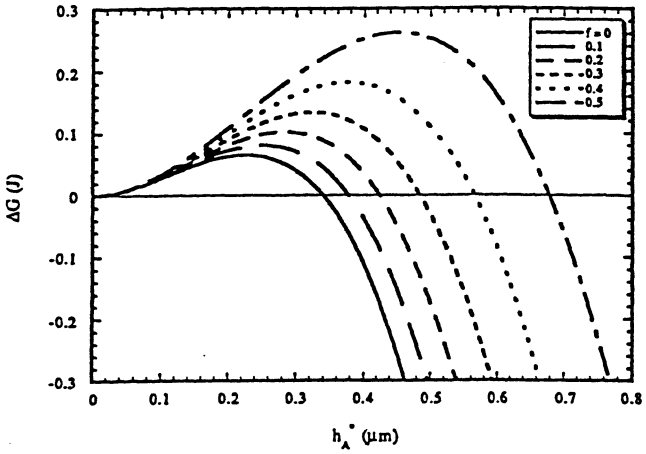

Fig. 11—ΔG as a function of h_A and f; E = 350 GPa, ν = 0.2, and γ = 1 J/m^2.

lated to the principal strains in linear elasticity by the relationship[33]

$$\sigma_{11} = \sigma_{22} = \left(\frac{E}{1-\nu}\right) \varepsilon_{11} \qquad [19]$$

where E is the Young's modulus, ν is Poisson's ratio, ε_{11} is the principal strain within the plane of the TiC_x layer, and σ_{11} is the principal stress associated with ε_{11}. For a plane state of stress, the strain energy density is simply $\sigma_{11}\varepsilon_{11}$, where σ_{11} is given by Eq. [19]. Thus, the strain energy density is given by

$$w_0 = \sigma_{11}\, \varepsilon_{11} = \left(\frac{E}{1-\nu}\right) \varepsilon_{11}^2 \qquad [20]$$

To calculate the strain energy density w_0, it is assumed that the stoichiometric coefficient x within the TiC_x layer varies linearly from 0.96 at the C/TiC_x interface to 0.47 at the TiC_x/Ti-Ni melt interface and does not vary with time. The stoichiometric coefficient is given by

$$x = -0.49 \left(\frac{z}{h_A^*}\right) + 0.96 \qquad [21]$$

where z is the spatial coordinate perpendicular to the plane of the TiC_x layer. The variation of strain in the TiC_x layer is given by

$$\varepsilon_{11} = \frac{a_x - a_0}{a_0} \qquad [22a]$$

$$\varepsilon_{11} = 7.15 \times 10^{-3} + 5.2 \times 10^{-4} \left(\frac{z}{h_A^*}\right) - 4.33 \times 10^{-3} \left(\frac{z}{h_A^*}\right)^2 - 3.35 \times 10^{-3} \left(\frac{z}{h_A^*}\right)^3 \qquad [22b]$$

Equation [22b] was obtained by fitting the nonstoichiometric lattice parameter a_x in Eq. [22a] and shown in Figure 8 with a third-order polynomial (a_0 = 0.43 nm[26]). The variation of stress within the TiC_x layer is obtained by combining Eq. [22b] with [19], assuming that the elastic moduli do not vary with stoichiometry. Figure 10 shows the variation of stress within the TiC_x layer as a function of its Young's modulus E and Poisson's ratio ν = 0.2. Consistent with this model, the maximum compressive stress is at the C/TiC_x interface. In order to calculate the average strain energy density $\bar{w}_0$, Eq. [22b] must be combined with Eq. [20] and then integrated over the thickness of the layer. Because the variation of C concentration was chosen to be linear throughout the TiC_x layer, the average strain energy density of the TiC_x layer is independent of its thickness h_A (it only depends upon the elastic constants). The average strain energy density is given by

$$\bar{w}_0 = \frac{1}{h_A^*} \int_0^{h_A^*} \sigma_{11}\, \varepsilon_{11}\, dz = \frac{1}{h_A^*} \left(\frac{E}{1-\nu}\right) \int_0^{h_A^*} \varepsilon_{11}^2\, dz$$

$$\bar{w}_0 = (2.585 \times 10^{-5}) \left(\frac{E}{1-\nu}\right) \qquad [23]$$

Combining Eq. [23] with [17] yields the difference in free energy between configurations 1 and 2 in Figure 9 as a function of layer thickness h_A, residual strain energy f, Young's modulus E, and Poisson's ratio ν. Figure 11 shows the variation of ΔG with h_A, f, E = 350 GPa, and ν = 0.2. The room-temperature Young's modulus of stoichiometric TiC is approximately 450 GPa.[34] For this model, it was assumed that the elastic moduli are independent of stoichiometry and temperature. However, this is not true, since it is known that the major contributors to the bond strength of TiC are the covalent Ti-C bonds which themselves increase with increasing C concentration and decrease with temperature because their equilibrium atomic spacing increases.[35,36] Thus, E = 350 GPa is the estimated value of the Young's modulus near the adiabatic temperature. For $h_A < h_A^*$, the free energy of configuration 2 is greater than that of configuration 1. This is due to the larger surface energy per unit volume of material for configuration 2. For $h_A > h_A^*$, the free energy of configuration 2 is less than that of configuration 1. Thus, if it is kinetically possible, the morphology of configuration 1 would change to a configuration with a lower free energy. If the assumption that the TiC_x layer which forms as a result of the reaction between the Ti-Ni-C melt and C particle is elastically strained due to compositional variation, configuration 2 represents a lower free energy state than configuration 1 for $h_A > h_A^*$, and the minimization of strain energy is the driving "force" for the morphological change.

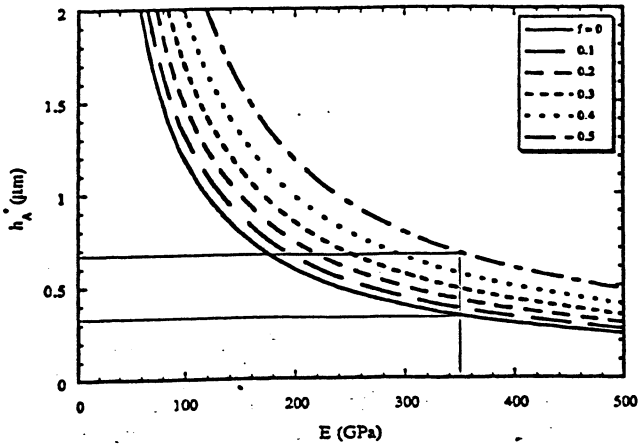

Fig. 12—Variation of critical thickness h_A^* with E and f; $\nu = 0.2$ and $\gamma = 1$ J/m².

From Equation [18], the critical thickness h_A^* is inversely proportional to the Young's modulus of the layer.

$$h_A^* = 1.484 \times 10^5 \left[\frac{1-\nu}{(1-f)E}\right]\gamma \qquad [24]$$

Figure 12 shows the variation of critical thickness h_A^* with Young's modulus E, f, and $\nu = 0.2$. It can be seen that compliant layers (*i.e.*, low Young's modulus) can grow to a thickness of several microns before they become thermodynamically unstable. The critical thicknesses h_A^* from Figure 12 for $E = 350$ GPa and $f = 0$ and 0.5 are approximately 0.34 and 0.68 μm, respectively. This is consistent with the size of both the TiC_x layer thickness and initial TiC_x spherule size, as seen in Figures 7(b) and 8(a) of the companion article.[1]

While the preceding model is able to predict the critical thickness at which the TiC_x layer is unstable relative to the formation of TiC_x spherules, which is consistent with observation, the actual driving force and mechanism by which the TiC_x layer breaks up and separates into the TiC_x spherules have not been identified. The extent to which the growth and morphology of individual TiC_x grains within the layer, as well as their separation from the layer, are affected by the reaction, diffusion of C and Ti (*i.e.*, surface and bulk), local stresses due to compositional variation and differences in thermal expansion behavior, and interfacial surface energies is not known. However, it is most likely that one or a combination of these processes results in the formation of these TiC_x spherules either directly or indirectly. The mechanism is analogous to the one recently observed and studied by Vecchio *et al.*[37] and Meyers *et al.*[38] for $NbSi_2$. In the latter case, however, the product phase is formed in the liquid state, whereas the formation of the TiC_x spherules is a solid-state process.

IV. CONCLUSIONS

An apparent activation energy of 120 ± 40 kJ/mol was obtained which, in accordance with Kirdyashkin *et al.*[17] and Dunmead *et al.*,[18] corresponds to the activation energy for C dissolution into the Ti-Ni-C melt. A simple model based upon C diffusion through TiC as the rate-limiting mechanism of reaction predicts that for C particles less than 0.23-μm thick, the time of C consumption will be less than 0.2 seconds; the C particles used in this study had thicknesses below this value.

The principal characteristics of the mechanism of reaction and formation of the TiC_x spherules are shown in Figure 2. The formation of solid TiC_x layers surrounding the C particles and their subsequent morphological evolution into TiC_x spherules ensures a high rate of reaction. Two mechanisms of formation of the TiC_x layer are discussed: (a) dissolution reprecipitation and (b) reaction diffusion. The relative values of the diffusion coefficients (diffusion of C in TiC_x is several orders of magnitude greater than diffusion of Ti) lead to ruling out the second mechanism.

Calculations were carried out assuming that the morphological evolution is dominated by the minimization of strain energy within the layer. Given the relatively high growth rates of the layers, stress relaxation due to diffusional or dislocation motion processes was neglected. Chiu and Gao[30] have shown that the formation of cusps of a critical wavelength in an initially flat layer under stress leads to an overall reduction in the energy of the system, the increase in interfacial energy being outweighed by the decrease in strain energy. On this basis, a simple model was developed to predict the critical thickness of the TiC_x layer (strain energy generated within the layer due to compositional variation) at which spontaneous formation of the TiC_x spherules would lead to an overall lowering of the energy of the system. Assuming a Young's modulus of 350 GPa, a Poisson's ratio of 0.2, and no residual strain energy yields a critical thickness of 0.34 μm. Within an order of magnitude, this value is consistent with the observed result.[1]

ACKNOWLEDGMENTS

This research was supported by the United States Army Research Office under Contract Nos. ARO-DAAL-03-88-K-0194 and ARO-DAAL-03-90-G-0204 and by the National Science Foundation under Grant No. CBT-8713258, DMR-8713258, DMR-9116570, and DMR-9396132. We thank the continued support of Drs. E.S. Chen and A. Crowson. Support by the Institute for Mechanics and Materials, Dr. Richard Skalak, Director, is greatly appreciated. Discussions with Drs. A. Strutt and A. Niiler were very informative.

REFERENCES

1. J.C. LaSalvia, D.K. Kim, R.A. Lipsett, and M.A. Meyers: *Metall. Mater. Trans. A*, 1995, vol. 26A, pp. 3011-3019.
2. A.S. Rogachev, A.S. Mukas'yan, and A.G. Merzhanov: *Dokl. Akad. Nauk SSSR*, 1987, vol. 297, pp. 1240-43.
3. A.S. Rogachev, V.M. Shkiro, I.D. Chausskaya, and M.V. Shvetsov: *Comb. Expl. Shock Waves*, 1988, vol. 24, pp. 720-26.
4. A.G. Merzhanov, A.S. Rogachev, A.S. Mukas'yan, and B.M. Khusid: *Comb. Expl. Shock Waves*, 1990, vol. 26, pp. 92-102.
5. A.M. Bulaev, S.V. Vedeneev, L.M. Buchatskii, and Yu. A. Gal'chenko: *Comb. Expl. Shock Waves*, 1990, vol. 26, pp. 198-201.
6. A.S. Mukasyan and I.P. Borovinskaya: *Int. J. Self-Prop. High-Temp. Syn.*, 1992, vol. 1, pp. 55-63.
7. A.G. Merzhanov and A.S. Rogachev: *Pure Appl. Chem.*, 1992, vol. 64, pp. 941-53.
8. B.M. Vol'ne and V.V. Evstigneev: *Combust. Expl. Shock Waves*, 1992, vol. 28, pp. 173-78.

9. E.A. Levashov, Yu.V. Bogatov, A.S. Rogachev, A.N. Pityulin, I.P. Borovinskaya, and A.G. Merzhanov: *J. Eng. Phys. Thermophys.*, 1992, vol. 63, pp. 1091-1105.
10. I.P. Borovinskaya, E.A. Levashov, and A.S. Rogachev: *Physical-Chemical and Technological Base of Self-Propagating High-Temperature Synthesis: Course of Lectures*, Scientific-Educational Center of SHS, Moscow, 1991.
11. A.A. Zenin, A.G. Merzhanov, and G.A. Nersisyan: *Dokl. Akad. Nauk SSSR*, 1980, vol. 250, pp. 83-87.
12. T. Boddington, P.G. Laye, J.R.G. Pude, and J. Tipping: *Comb. Flame*, 1982, vol. 47, pp. 235-54.
13. T. Boddington, P.G. Laye, J. Tipping, and D. Whalley: *Comb. Flame*, 1986, vol. 63, pp. 359-68.
14. B.V. Novozhilov: *Dokl. Acad. Sci. USSR, Phys. Chem.*, 1961, vol. 141, pp. 836-38.
15. E.I. Maksimov, A.G. Merzhanov, and V.M. Shkiro: *Combust. Expl. Shock Waves*, 1965, vol. 1, pp. 15-18.
16. A.G. Merzhanov: *Comb. Flame*, 1969, vol. 13, pp. 143-56.
17. A.I. Kirdyashkin, Yu.M. Maksimov, and E.A. Nekrasov: *Combust. Expl. Shock Waves*, 1977, vol. 17, pp. 377-79.
18. S.D. Dunmead, D.W. Readey, and C.E. Semler: *J. Am. Ceram. Soc.*, 1989, vol. 73, pp. 2318-24.
19. D.A. Porter and K.E. Easterling: *Phase Transformations in Metals and Alloys*, Chapman and Hall, London, 1981.
20. S. Sarian: *J. Appl. Phys.*, 1969, vol. 40, pp. 3515-20.
21. S. Sarian: *J. Appl. Phys.*, 1968, vol. 39, pp. 3305-10.
22. P. Shewmon: *Diffusion in Solids*, 2nd ed., TMS, Warrendale, PA, 1989.
23. *Binary Alloy Phase Diagrams*, T.B. Massalski, ed., ASM, Metals Park, OH, 1986, vol. 1.
24. M.E. Fine: *Introduction to Phase Transformations in Condensed Systems*, MacMillan, New York, NY, 1964, pp. 33-43.
25. E.R.G. Eckert and R.M. Drake, Jr.: *Analysis of Heat and Mass Transfer*, McGraw-Hill Book Company, New York, NY, 1972.
26. E.K. Storms: *The Refractory Carbides*, Academic Press, New York, NY, 1967.
27. *CRC Handbook of Chemistry and Physics*, D.R. Lide, ed., CRC Press, Boston, MA, 1990.
28. M.W. Chase, Jr., C.A. Davies, J.R. Downey, Jr., D.J. Frurip, R.A. McDonald, and A.N. Syverud: *JANAF Thermochemical Tables*, 3rd ed., parts I and II; *J. Phys. Chem. Ref. Data*, 1985, vol. 14, suppl. 1, American Chemical Society and American Institute of Physics for the National Bureau of Standards, Washington, D.C., 1986.
29. J.Y. Tsao: *Materials: Fundamentals of Molecular Beam Epitaxy*, Academic Press, New York, NY, 1993.
30. C.H. Chiu and H. Gao: *Int. J. Solids Struct.*, 1993, vol. 30, pp. 2983-3012.
31. N. Grandjean and J. Massies: *J. Cryst. Growth*, 1993, vol. 134, pp. 51-62.
32. *Cermets*, J.R. Tinklepaugh and W.B. Crandall, eds., Reinhold Publishing Corporation, New York, NY, 1960.
33. Y.C. Fung: *Foundations of Solid Mechanics*, Prentice-Hall, Englewood Cliffs, NJ, 1965.
34. L.E. Toth: *Transition Metal Carbides and Nitrides*, Academic Press, New York, NY, 1971.
35. G.S. Pisarenko, V.N. Rudenko, G.N. Tret'yachenko, and V.T. Troshchenko: *High-Temperature Strength of Materials*, Israel Program for Scientific Translations Ltd., Jerusalem, 1969.
36. G. Grimvall: *Thermophysical Properties of Materials*, North-Holland, New York, NY, 1986.
37. K.S. Vecchio, L.H. Yu, and M.A. Meyers: *Acta Metall. Mater.*, 1994, vol. 42, pp. 701-14.
38. M.A. Meyers, L.H. Yu, and K.S. Vecchio: *Acta Metall. Mater.*, 1994, vol. 42, pp. 715-29.